PERGAMON

Available online at www.sciencedirect.com
SCIENCE DIRECT®

Continental Shelf Research 23 (2003) 1019–1034

CONTINENTAL SHELF RESEARCH

www.elsevier.com/locate/csr

Observations of infragravity wave frequency selection

Troels Aagaard[a,*], Karin R. Bryan[b,1]

[a] *Institute of Geography, University of Copenhagen, Øster Voldgade 10, DK-1350 Copenhagen, Denmark*
[b] *National Institute for Water and Atmospheric Research Ltd. (NIWA), Hamilton, New Zealand*

Received 4 May 2001; received in revised form 6 March 2003; accepted 14 April 2003

Abstract

Field measurements of sea-surface elevation, cross-shore and longshore velocities were obtained during a storm event on the north coast of Zealand, Denmark from a cross-shore array of co-located pressure sensors and current meters. During the major part of this storm, statistically significant spectral peaks at a frequency of $f \approx 0.025$ Hz were identified at several cross-shore locations. Based on examinations of cross-shore coherence and phase relationships, it appeared that these motions were due to cross-shore standing wave structures rather than caused by shear wave activity. Comparisons with synthetic edge wave spectra, which were computed assuming a white shoreline surface elevation spectrum, suggested that the identified spectral peaks were not artifacts of a cross-shore standing wave nodal structure but an indication that those frequencies where the peaks occurred were preferentially forced. Analyses of local and spatial phase relationships of velocity and sea-surface elevation, as well as comparisons with numerically calculated theoretical cross-shore wave structures suggested that these waves were standing edge waves with mode number $(n) \geqslant 3$. The selected frequency of $f \approx 0.025$ Hz corresponds to one of the cut-off frequencies that can theoretically occur on this bathymetric geometry which asymptotes to a constant depth offshore.

PACS: Denmark; Zealand; Kattegat

Keywords: Infragravity waves; Edge waves; Coastal oceanography; Beaches; Beach morphodynamics; Nearshore bars

1. Introduction

The presence of cross-shore standing infragravity waves in the nearshore zone has been recognized for many years (e.g. Munk, 1949). Such waves generally have frequencies between ≈ 0.005 and 0.05 Hz and may be either edge waves which are trapped against beaches (Eckart, 1951) or across nearshore bars (Kirby et al., 1981; Bryan and Bowen, 1996) by refraction and reflection, or they may be leaky mode waves that radiate energy back offshore.

The interest in cross-shore standing infragravity wave motions is partly due to the fact that they may transport significant amounts of sediment (Beach and Sternberg, 1991; Russell, 1993; Aagaard and Greenwood, 1994) and potentially play a significant role in surf zone morphodynamics. Theoretical considerations show that

*Corresponding author. Fax: +45-3532-2501.
E-mail address: taa@geogr.ku.dk (T. Aagaard).
[1] Now at Department of Earth Sciences, University of Waikato, Hamilton, New Zealand.

0278-4343/03/$ - see front matter
doi:10.1016/S0278-4343(03)00082-7

discrete-mode, cross-shore standing infragravity waves possess a well-defined cross-shore structure with a series of offshore nodes and antinodes. Consequently, they have been hypothesized to account for the generation of nearshore bars (Short, 1975; Bowen, 1980) with bar crests at surface elevation antinodes where drift velocities at the top of the bottom boundary layer converge. Rhythmic morphologies could conceivably be due to longshore-standing edge wave motions (Bowen and Inman, 1971; Holman and Bowen, 1982).

The existence and hydrodynamic significance of infragravity edge waves in the surf zone was proven conclusively by, e.g. Huntley et al. (1981), Oltman-Shay and Guza (1987) and Howd et al. (1991). Edge waves are particularly important during high-energy conditions as their amplitudes appear to be linearly related to offshore incident wave heights (Guza and Thornton, 1982; Herbers et al., 1995; Ruessink, 1998). A major concern, however, in any practical evaluation of the capability of standing infragravity waves to impose spatially segregated sediment transport patterns and thus bar growth and/or migration is whether the waves are sufficiently energetic and whether they have a reasonably well-defined cross-shore (and/or longshore) structure. In other words, discrete and spatially coherent modes and frequencies must dominate the low-frequency velocity field; certain frequency/mode combinations must be preferentially forced. Furthermore, given the fact that any morphological response lags the hydrodynamic forcing, these discrete modes and frequencies should persist for a significant length of time during a high-energy event.

Discrete edge wave modes and frequencies can occur theoretically when a sloping shoreface profile displays a profile discontinuity, seaward of which the slope becomes zero. Edge waves whose cross-shore extent matches the cross-shore length scale of the sloping profile segment were thought to become preferentially amplified and were termed cut-off modes (Ursell, 1952; Huntley, 1976).

However, discrete-frequency infragravity waves have rarely been observed in the field. Under natural conditions, the infragravity wave band is often broad with no particular frequencies/modes being dominant (Guza and Thornton, 1985; Oltman-Shay and Guza, 1987; Ruessink et al., 1998; Holland and Holman, 1999). A few studies from enclosed seas or lakes have provided some indications of frequency selection (Aagaard, 1990; Bauer and Greenwood, 1990). However, the amount of data from these latter experiments was limited and observations from surf zones may be ambiguous as the nodal structure of a broad-banded standing wave field will produce artificial peaks and valleys in velocity and surface elevation spectra at discrete locations away from the shoreline.

This paper reports on a field experiment during which measurements of sea surface elevation and cross-shore and longshore velocities were obtained at eight cross-shore positions during a storm at the north coast of Zealand, Denmark. The cross-shore profile shape at the site approximates the shape required by the cut-off hypothesis and during the storm, observed infragravity wave spectra became distinctly peaky. Infragravity wave frequency selection will be investigated by comparing measured spectra with model predictions that were made assuming a white shoreline spectrum. The type of wave motion will be examined by comparing data with theoretically predicted cross-shore wave structures and finally observed peak spectral frequencies will be compared with theoretically predicted cut-off frequencies.

2. Theoretical background

For edge waves travelling along a longshore homogeneous topography such that

$$\eta(x, y, t) = \eta(x)e^{i(\omega t - k_y y)}, \tag{1}$$

where η is the sea-surface elevation, x is cross-shore distance, ω is edge wave radian frequency and k_y is longshore radian wave number, the linear, irrotational, inviscid shallow water equations can be combined to yield the edge wave equation

$$\left(\frac{gh\eta_x}{\omega^2}\right)_x + \left(1 - \frac{k_y^2 gh}{\omega^2}\right)\eta = 0 \tag{2}$$

and

$$u = \frac{-\mathrm{i}g}{\omega}\eta_x$$
$$v = \frac{gk_y}{\omega}\eta \quad (3)$$

where h is water depth, η_x is the cross-shore distribution of sea-surface elevation, u is cross-shore orbital velocity, v is longshore orbital velocity and g is the acceleration due to gravity. The x-dependencies of η, u and v in Eqs. (2) and (3) are understood.

For simple topographies, for example a planar slope (Eckart, 1951) or an exponential profile (Ball, 1967), Eq. (2) can be solved analytically to yield the edge wave dispersion relation. For more complex topographies, however, Eq. (2) must be solved numerically (Holman and Bowen, 1979), for example by using the model outlined by Howd et al. (1992) and Bryan and Bowen (1996).

Howd et al. (1991, 1992) demonstrated that the presence of a strong longshore current produces a similar effect on the edge wave shape as a change in the depth profile. This effective depth can be related to the true depth by

$$h'(x) = \frac{h(x)}{\left(1 - V(x)/C\right)^2} \quad (4)$$

where V is longshore current velocity and C is edge wave celerity (ω/k_y). Eq. (2) is then modified to

$$\left(\frac{gh\eta_x}{(-\omega + k_y V)^2}\right)_x + \left(1 - \frac{k_y^2}{(-\omega + k_y V)^2}\right)\eta = 0 \quad (5)$$

Eqs. (2) and (5) give an indication of the frequency and wave number that an hypothetical edge wave would have on a particular bathymetry, but they do not give any indication of which frequencies and modes will be energetic on a particular beach. For example, would one expect edge waves to occur at a range of frequencies, or does frequency selection, i.e. preferential amplification of certain frequencies/modes occur?

Infragravity waves can be forced by non-linear interactions between incident wind wave pairs in shallow water which produce temporally and spatially alongshore varying gradients in radiation stress at the same time and length scale as the infragravity waves (Longuet-Higgins and Stewart, 1962; Gallagher, 1971; Bowen and Guza, 1978). If such radiation stress gradients satisfy the edge wave dispersion relation, the response will be a resonantly excited edge wave trapped against a sloping beach. Symonds et al. (1982) and Lippmann et al. (1997) showed that infragravity response could be due to the wave group-induced modulation in breakpoint position and the resulting temporally and spatially varying momentum fluxes. If the pattern in the radiation stress gradients at the breakpoint varied at edge wave wave numbers and frequencies, energy would be transferred from the incident waves to the edge waves. The forcing of a particular edge wave becomes a linear sum of all possible interactions satisfying the edge wave dispersion relationship (Lippmann et al., 1997).

A number of reasons have been proposed to explain why one frequency/mode can be selected over another. The simplest, yet most unlikely, is that only two single, essentially monochromatic incident wave trains exist. More plausible explanations centre on the bathymetry causing more generalized forcing conditions to select certain frequencies and modes. One such argument is given by Symonds and Bowen (1984) who showed that even in the case of broad-banded forcing, edge waves with surface elevation antinodes over bars should tend to become preferentially selected, thus potentially providing a mechanism for bar stability and growth.

In a similar vein, when considering a beach with a planar slope extending some distance offshore and terminating at a slope break at $x = x_0$, beyond which the slope becomes zero, Ursell (1952) and Huntley (1976) suggested that edge waves may be preferentially amplified when the longshore wave number of an edge wave becomes equal to the wave number of a free gravity wave at $x > x_0$ (corresponding to $C = (gh_0)^{\frac{1}{2}}$, where h_0 is water depth seaward of the slope break). Combinations of wave radian frequencies and wave numbers (ω, k_y) corresponding to $(gh_0)^{\frac{1}{2}}$ were named cut-off modes. The cause for their selective amplification may be that edge waves whose cross-shore length scale is small relative to the width of the nearshore could be discriminated against by surf zone damping (i.e. turbulence due to wave breaking;

Bowen and Guza, 1978). On the other hand, waves having $C > (gh_0)^{\frac{1}{2}}$ are oscillatory over the h_0 region; these waves are leaky waves and radiate energy offshore (Guza and Inman, 1975). Alternatively, Ursell (1952) suggested that cut-off mode edge waves remain trapped in the nearshore and become particularly strongly resonant due to the effects of viscosity.

3. Field site

The field experiment was conducted at Staengehus on the northern coast of Zealand, Denmark during October–November 1998. The average nearshore slope is approximately $\beta = 0.016$ and the site has three longshore bars (Fig. 1). Seaward of the outer bar, at $x \approx 500$ m, there is a distinct profile discontinuity seaward of which the nearshore slope becomes very small, $\beta \approx 0.0025$. The two inner bars are mobile during storm events and they are frequently characterized by rhythmic bar topographies while the outer bar is generally linear and considerably more stable in position (Aagaard, 1990). The mean sand grain size on the bars is approximately 200–250 μm microns while troughs between bars often constitute zones of erosion where the sand has been winnowed away and gravels and cobbles are exposed (Figs. 1 and 2). Seaward of the profile discontinuity, the seabed is composed of till with scattered patches of sand.

The wave climate at the site is highly variable. As the beach is exposed towards the direction of the strongest winds and fetches are relatively short

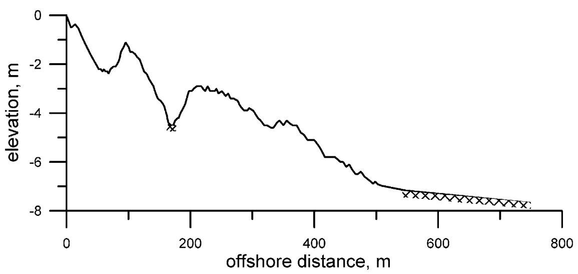

Fig. 1. Cross-shore profile at the research site, surveyed October 13, 1998. The cross-hatched signature indicates areas where till and/or cobbles were exposed.

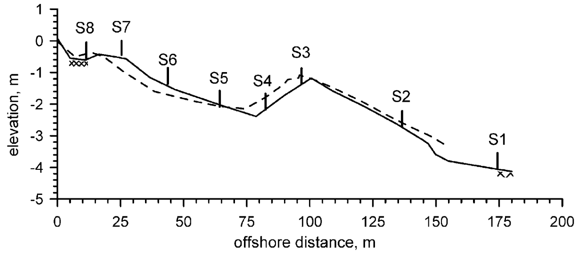

Fig. 2. Cross-shore profiles of the inner nearshore surveyed prior to the storm (October 13; solid line) and at the end of the experiment (October 24; dashed line). Positions and designations of instrument stations are indicated. The cross-hatched signature indicates areas where till and/or cobbles were exposed.

($\leqslant$150 km), brief storm events with breaker heights over the outer bar up to 2–2.5 m and peak spectral wave periods of 5–7 s are interspersed with lengthy and relatively calm periods. Long-period swell energy is insignificant and the tidal range is very small, on the order of 0.2–0.3 m.

4. Sensor deployment

Eight instrument stations were established in a cross-shore transect across the inner and middle bars and designated S1–S8 (Fig. 2). The stations were deployed at quasi-uniform intervals in order to achieve a reasonably consistent spatial coverage relative to the existing bathymetry and they were each equipped with a Viatran Model 240 pressure transducer and a single Marsh-McBirney OEM512 electromagnetic current meter except for stations S4 which had only a current meter and S8 which had only a pressure sensor. The current meters were installed at elevations of 0.2–0.25 m above the bed along with arrays of optical backscatter sensors (D&A Instruments OBS-1P) for suspended sediment transport measurements. The sensors were hardwired to a shore-based PC data-acquisition system and sampled at 10 Hz for 45 min intervals with a duty cycle of 1 h during storm events. Pressure sensors and current meters were calibrated prior to deployment. Field offsets were checked repeatedly in buckets and during still water conditions.

All time series were subjected to visual inspection to ensure data quality. At times, particularly during the beginning of storm events, problems were encountered with seaweed becoming entangled around sensors. This resulted in diminishing and/or sudden changes in current meter outputs along with varying offsets and/or signal saturation of optical backscatter sensors; such records were omitted from further analysis.

5. Observations

The storm event reported here occurred on October 14–16, 1998, corresponding to experimental hours 212–264. At the onset of the storm, significant wave heights at the seaward slope of the middle bar increased from ~0.4 m to 1.1 m and later reached a maximum of 1.7 m during hour 254 (Fig. 3). Peak spectral wave periods increased from 4.0 to 6.9 s and the mean angle of wave incidence was 12–22°. At times of maximum wave energy, waves broke over the outer bar, reformed in the trough and broke almost continuously from the seaward slope of the middle bar to the shoreline (Fig. 4). Infragravity wave heights (summed over all frequencies <0.067 Hz) were on the order of 0.2–0.25 m and almost constant across the inner part of the surf zone with slight amplifications over bar crests, an effect which was also observed by Lippman et al. (1999). Mean currents were directed offshore and to the northeast; maximum observed cross-shore currents on the crest of the middle bar were 0.39 m/s and longshore currents peaked at 0.82 m/s during hour 246 (Fig. 3). The cross-shore distribution of longshore current velocities during the initial stages and peak of the storm is illustrated in Fig. 5 which consistently displays two longshore current jets over the middle and inner bars with longshore current minima in the troughs. Tidally induced changes of the mean water depth were small, but the storm generated a superelevation of the water level of approximately 0.60 m due to the wind surge (Fig. 3).

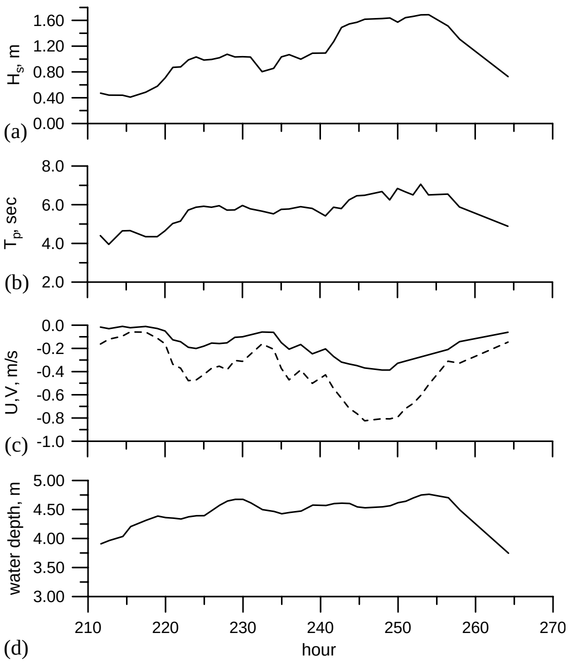

Fig. 3. Significant wave height (a) and peak spectral wave period (b) at S2 close to the breakpoint, (c) mean cross-shore (solid line) and longshore (dashed line) current velocities at the bar crest (S3), and (d) water depth recorded at the seawardmost station (S1) through the storm event.

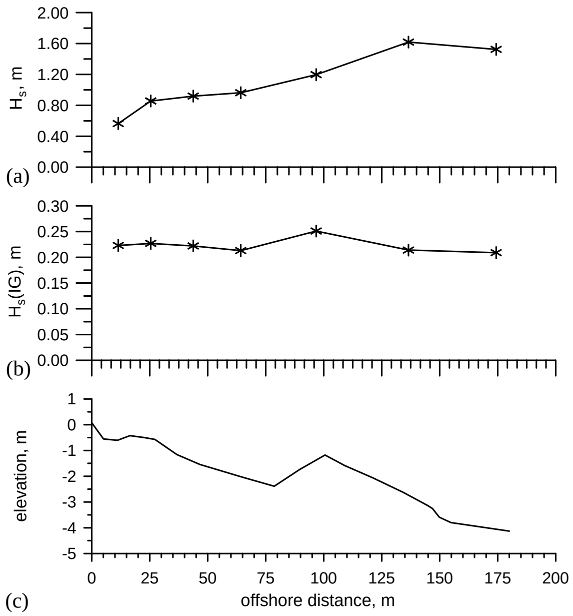

Fig. 4. (a) Total significant wave height and (b) significant infragravity wave height measured across the instrument array during the storm peak (hour 246). The profile is shown in panel (c).

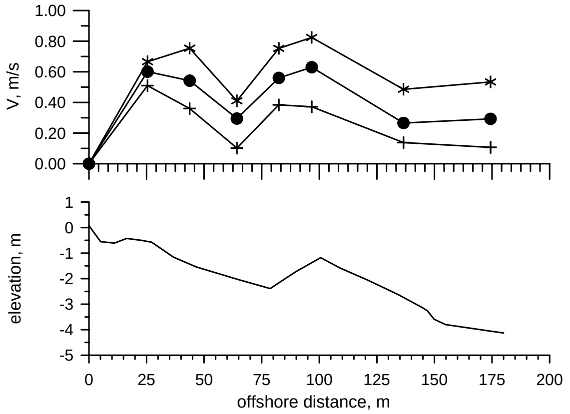

Fig. 5. The cross-shore distribution of longshore currents during hour 235 (+), hour 243 (•) and hour 246 (∗). Note the consistent cross-shore shape of the velocity profile with only small displacements of longshore current maxima.

During the storm peak (hours 239–258) statistically significant infragravity peaks appeared in several of the spectra of surface elevation and velocity at a frequency of $f = 0.024$–0.025 Hz. Given the relatively uniform cross-shore spacing between sensor positions, an attempt was made to compute surf zone averaged infragravity spectra by averaging all recorded spectra on a frequency-by-frequency basis, in the frequency band $f = 0$–0.050 Hz. In the examples illustrated in Fig. 6, recorded 7 h apart, energy at $f = 0.024$–0.025 Hz dominated the averaged spectra of surface elevation. With respect to cross-shore velocities, energy at these frequencies was also high but exceeded by energy at very low frequencies, <0.010 Hz.

In an investigation of standing infragravity wave motions, it is necessary to avoid analysing frequencies which are contaminated by shear wave motions. The fact that the $f \approx 0.025$ Hz peak is clearly evident in the surface elevation spectra (Fig. 6a) suggests that this energy was not due to shear waves. In the absence of longshore instrument arrays, a further method to identify whether wave motions at discrete frequencies are due to cross-shore standing infragravity wave motion involves an analysis of cross-shore coherence and phase structures. Standing infragravity motions should display a relatively high level of coherence across the instrument array with cross-shore phases close to 0 or 180° whereas, e.g. shear wave

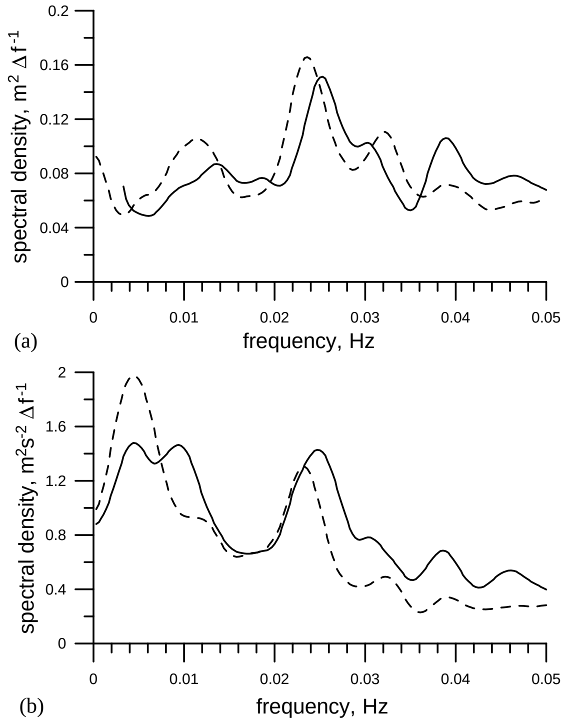

Fig. 6. Surf zone-averaged spectra of (a) surface elevation and (b) cross-shore velocity. Hour 246 (solid lines) and hour 253 (dashed lines).

motions would be expected to be considerably less coherent, particularly given the longshore current structure depicted in Fig. 5, showing two individual current maxima at the inner and middle bars. Furthermore, shear wave motions should lack the 180° phase shifts induced by standing wave nodal positions. Cross-spectra of cross-shore velocity were computed between stations S7 and S2 in the inner and outer parts of the array, again for the two instrument runs used in Fig. 6. Examining Fig. 7, cross-shore coherence displayed prominent peaks in coherence at $f = 0.024$–0.025 Hz with phases close to 180° whereas coherence was not, or only marginally significant in the frequency band $f = 0.00$–0.01 Hz and phases were random. Spatial phase relationships of cross-shore velocity and surface elevation were also examined across the entire array. Fig. 8 illustrates an example of surface elevation phase relationships relative to station S5, and cross-shore velocity phases relative to station S7 at $f = 0.010$ Hz and $f = 0.025$ Hz for hour 246 during the storm peak. At $f = 0.025$ Hz, phases were consistently close to 0° or 180° which is indicative of cross-shore standing wave motions. With respect to cross-shore velocity, the phase jumps indicate a node (i.e. a surface elevation antinode) close to station S4 and there are

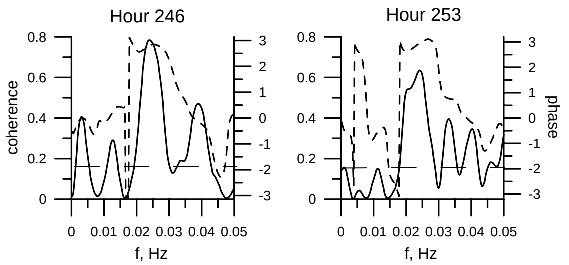

Fig. 7. Spatial coherence (solid lines) and phases (dashed lines) between stations S2 and S7. The horizontal dashed lines indicate the 99% confidence level on coherence.

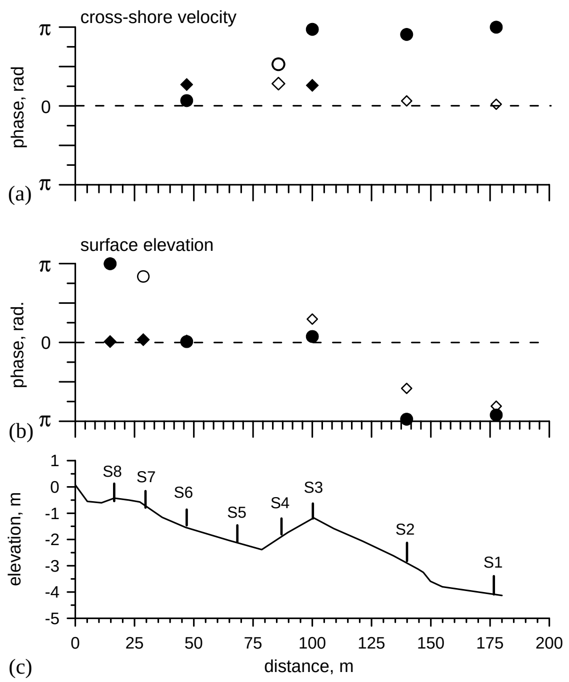

Fig. 8. Cross-spectral phase relationships of cross-shore velocity relative to S7 (a) and surface elevation relative to S5 (b) during hour 246 at $f = 0.010$ Hz (diamonds) and $f = 0.025$ Hz (circles). Filled diamonds/circles indicate statistically significant coherence at $\alpha = 0.01$. Bathymetric profile shown in panel (c) for comparison.

indications of surface elevation nodes between stations S6 and S7, and between stations S2 and S3. At $f = 0.010$ Hz, there is no indication of standing wave motion and coherence becomes insignificant with distance away from the reference sensors. It is therefore suggested that the peaks in Fig. 6b at frequencies $f = 0.00$–0.01 Hz were possibly due to shear wave motions, while the peaks at $f \approx 0.025$ Hz were due to cross-shore standing (infra)gravity motions.

The question then is whether the observed infragravity waves at $f \approx 0.025$ Hz (Fig. 6) were indeed preferentially selected, or whether the observed spectral peaks were artifacts of sensor position relative to a cross-shore standing wave structure. This can be examined by computing synthetic velocity/elevation spectra for given offshore instrument positions and assuming a white shoreline spectrum of unity surface elevation amplitude (Sallenger and Holman, 1987). Comparisons between such white-noise spectra and measured spectra should then reveal whether certain frequencies are preferentially amplified. Significant discrepancies should indicate a true (measured) spectral structure.

6. Model description and sensitivity

Synthetic spectra were produced using a numerical model for edge waves on arbitrary cross-shore bathymetry based on Eq. (5). The computer model systematically searches through frequency-wave number space to find frequency-wave number combinations that result in (edge wave) η- and u-profiles that decay to a user-selected tolerance level at the seaward end of the depth profile. The cross-shore η- and u-profiles are calculated using a Runge-Kutta numerical scheme. Dispersion properties produced by the model have been shown to consistently correspond to field observations of edge waves obtained from longshore arrays on both barred and planar beaches (Oltman-Shay and Guza, 1987; Howd et al., 1992; Oltman-Shay and Howd, 1993; Bryan et al., 1998; Bryan and Bowen, 1998).

Following Sallenger and Holman (1987), theoretical cross-shore velocity and surface elevation variances across the measured profile at a particular frequency were computed from

$$S_\eta(x) = \eta_n^2(x)$$
$$S_u(x) = \left(\frac{g}{\omega}\frac{\partial \eta_n}{\partial x}\right)^2 \quad (6)$$

where S_η, S_u are variances of sea-surface elevation and cross-shore velocity, respectively, n denotes the mode number and η_n is derived using the numerical model. We have assumed a white shoreline sea-surface spectrum in which surface elevation amplitude is constant for all modes and frequencies. Therefore, all peaks in the synthetic white-noise spectra output by the model at specific sensor locations are purely due to the nodal structure of the edge waves. If measured spectra exhibit peaks that are not predicted by the white-noise spectra, we can conclude that those peaks are not simply due to (broadbanded) edge wave nodal structure.

The predicted spectral shape at a given offshore position (for a white shoreline spectrum) will depend on mode number, bathymetry, changes in water depth and longshore current velocity. In Fig. 9, high-mode ($n = 4$) white-noise spectra have been computed for two different positions within the surf zone in order to assess the sensitivity of the model. In Fig. 9, panels (a) illustrate the effect of errors in estimated water depth and panels (b) show the effect of changing longshore currents, using the recorded longshore currents for hour 246 (Fig. 5), either following, or opposing an edge wave motion. Finally, panels (c) illustrate the effect of changing bathymetry by using the surveyed bathymetry immediately prior to, and 1 week after the storm (Fig. 2). These panels also illustrate the effects of longshore rhythmic bars. Edge wave shapes are expected to adjust to a longshore-averaged cross-shore profile and because the inner and middle bars at Staengehus were crescentic, the surveyed profiles may not be representative for such a longshore-averaged profile. The (onshore) shift in bar positions between the two surveys was on the order of 10 m; however, the rhythmic amplitude of the middle bar may be up to 15–20 m (Aagaard, 1990). Therefore, using the two surveyed profiles and a hypothetical profile similar to the October 13 profile but with the bars shifted 10 m seaward is considered to cover the likely range of longshore-averaged bathymetries for calculations of predicted spectra.

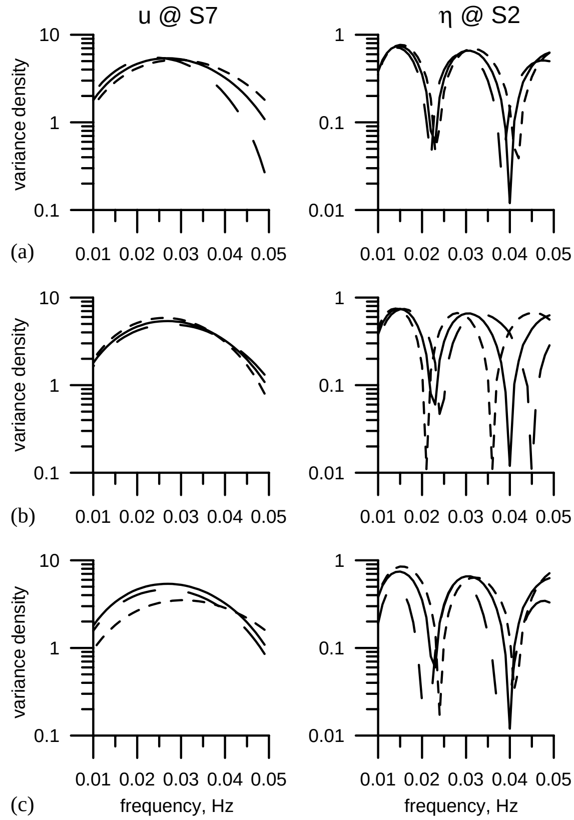

Fig. 9. Predicted spectral shapes for cross-shore velocity (u) at station S7 and surface elevation (η) at station S2, assuming a white shoreline spectrum of unity surface elevation amplitude. Panels (a) illustrate the effect of changes in water depth. The solid lines represent the recorded water depth, small dashes are for $+0.1$ m depth and large dashes are for -0.1 m depth. Panels (b) illustrate the effect of longshore currents (solid lines: no currents; small dash: opposing currents; large dash: following currents), using the October 13 bathymetry. Finally, panels (c) show predicted spectral shapes for the bathymetry of October 13 (solid lines) and October 24 (small dash) and the bathymetry of October 13 but with the bar shapes displaced 10 m seaward (large dash).

Close to the beach (i.e. at station S7; $x = 28$ m), errors associated with depth or longshore currents do not significantly change the shape of the predicted spectrum. There are no distinct spectral peaks or valleys in the white-noise spectrum, as this position is located landward of the first predicted cross-shore velocity node (for $n = 4$ edge waves and lower). Bathymetric errors and/or longshore-rhythmic bars do have some effect as the frequency of the maximum spectral density becomes somewhat displaced, but the overall spectral shape is not affected. Measurement errors will have more impact away from the shoreline (e.g. at S2; $x = 178$ m) as predicted spectral peaks and valleys shift slightly back and forth in frequency space. While errors in the directionality of the longshore current relative to edge wave propagation direction seem particularly critical, such errors again do not materially affect the overall shape of the predicted spectrum. Measurement errors particularly affect the higher frequencies.

In the following section, predicted white-noise spectra will be compared to the actually recorded spectral shapes at different cross-shore positions, while keeping in mind that the white-noise spectra will be less prone to input errors at the inner stations. The bathymetry prior to the storm event (i.e. October 13) with bars at intermediate positions will be used as well as recorded water depths while longshore currents will be ignored initially as it is difficult to assess a priori whether edge waves were propagating against, or with, the current.

7. Model-data comparisons

7.1. Spectral structure

Fig. 10a and b illustrate comparisons of measured and white-noise spectra of surface elevation and cross-shore velocity during the two example runs from the storm peak (hours 246 and 253). The white-noise spectra were again

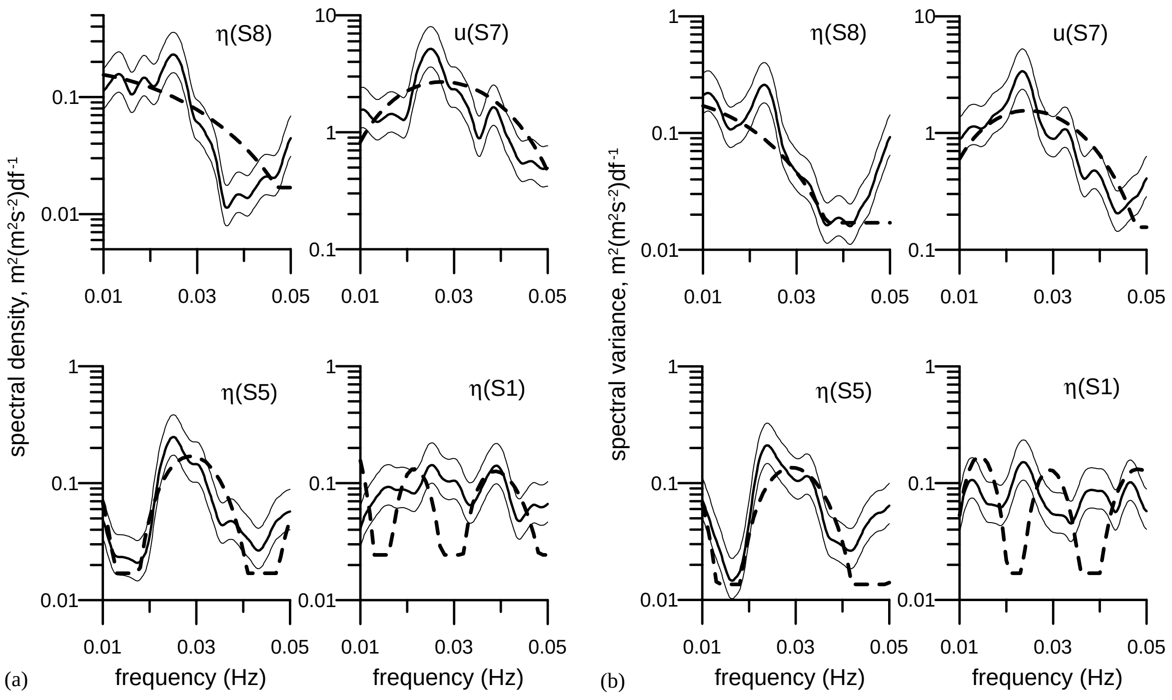

Fig. 10. (a) Measured (solid lines) and synthetic white-noise (dashed lines) infragravity wave spectra during hour 246 at S8 (surface elevation), S7 (cross-shore velocity), S5 (surface elevation) and S1 (surface elevation). Measured spectra have 50 degrees of freedom and the thin solid lines indicate the 95% confidence interval. Synthetic spectra were calculated for $n = 4$ edge waves on the October 13 bathymetry with no longshore currents. (b) As in Fig. 10 (a), but for hour 253.

computed for $n = 4$ edge waves and the comparisons are only illustrated for the stations where (measured) statistically significant spectral peaks were observed at $f \approx 0.025$ Hz. Sallenger and Holman (1987) shifted their white-noise spectra vertically to fit the lower energy peaks of the measured spectra. However, such an operation would appear to be rather subjective and in some cases not exactly straightforward as the predicted and measured spectral structure is sometimes very different. A more objective way to perform a comparison could be to scale the white-noise spectra to yield an equivalent variance between observed and synthetic spectra at frequencies $0.01 < f < 0.05$ Hz. The disadvantage using this method is that any instrument or system noise at spectral frequencies where there is no signal (i.e. at edge wave nodes) increases variance in the measured spectra and distorts the variance ratio between measured and synthetic spectra. To reduce this problem, a subjectively defined (but conservative) noise floor was added to the synthetic spectra, in which the noise floor was 10% of the peak spectral density. Examining the comparisons in Fig. 10a and b, it is evident that for the inner instrument stations (S8, S7), in particular, the measured spectral shape is very different from the predicted shape associated with a white shoreline spectrum. At these stations, measured spectra are distinctly peaky while a convex spectral shape without any peaks is predicted by the white-noise spectra because those instruments were landward of the first predicted surface elevation (S8) and/or velocity nodes (S7), respectively. The white-noise spectra, therefore, do not display the spectral peak/valley structure which is predicted for more offshore locations. The mere fact that distinct, statistically significant peaks were observed in measured spectra from S8 and S7 is indicative of frequency selection. Further offshore, peak frequencies in observed and synthetic spectra of surface elevation at S5 and S1 do not coincide and for hour 253, in particular, the statistically significant observed peak at $f = 0.024$ Hz is close to a nodal frequency for the white-noise spectrum.

These dominant infragravity wave motions persisted through the majority of the period of high wave energy. In Fig. 11, positive residuals between measured and predicted white-noise spectral density have been plotted for all instruments through the storm peak (hours 239–258). The residuals were computed as follows: First the white-noise spectrum was normalized by the total measured variance spectral density to produce the same amount of variance between $f = 0.01$ and 0.05 Hz as in the measured spectrum. Then the lower 95% confidence limit for the recorded spectrum was computed and finally, the (positive) absolute difference in spectral density between this confidence limit and the normalized white-noise spectrum was computed as a function of frequency. Only cases when this lower confidence limit exceeded the white-noise spectrum have been plotted; when white-noise variance exceeded the lower 95% confidence limit on the observed spectrum, the residual was assigned the value of zero. Hence, the spectral peaks depicted in Fig. 11 do not indicate absolute variance, but frequencies at which the measured spectrum contains more variance ($\alpha = 0.05$) than a white-noise spectrum containing the same total amount of variance between $f = 0.01$ and 0.05 Hz. Examining the 'excess-variance' spectra, it is evident that such positive residuals typically occurred within the frequency band $f = 0.02$–0.03 Hz, i.e. within the band containing the observed spectral peaks at $f = 0.024$–0.025 Hz. It is characteristic that positive residuals did not occur in both surface elevation and cross-shore velocity at the same instrument station, which is precisely what would be expected for a cross-shore standing wave structure. Positive residuals also often occurred at relatively high frequencies ($f = 0.04$–0.05 Hz) where the spectral density was, however, relatively low (Figs. 6 and 10). Based on the data presented in Figs. 10 and 11 and especially the fact that the observed spectral shapes were very different from white-noise spectra at the landward most stations, infragravity wave-frequency selection would appear to have occurred through the majority of the storm peak.

7.2. Cross-shore wave structure and wave type

In order to determine the type of observed wave motions at $f \approx 0.025$ Hz, model outputs of

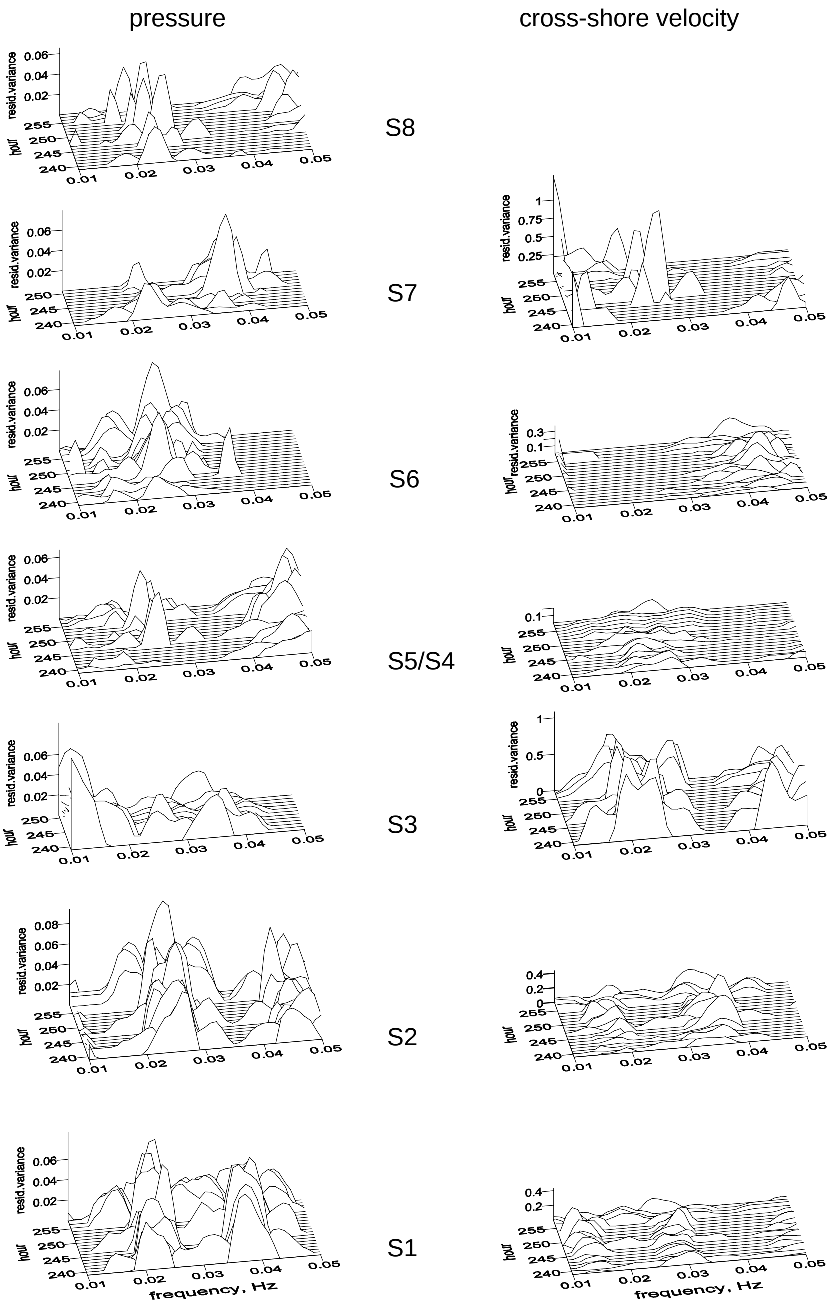

Fig. 11. Excess variance spectra of pressure (surface elevation) and cross-shore velocity at all stations during the storm peak (hours 239–258). The figures show the excess amount of variance in the measured spectra, relative to white-noise spectra containing the same total amount of variance in the infragravity band ($f = 0.01$–0.05 Hz).

cross-shore and longshore orbital velocity, as well as surface elevation profiles were plotted as a function of cross-shore distance and compared with the measured variance at the instrument stations. Water depths were adjusted to account for the actual water level and observed longshore

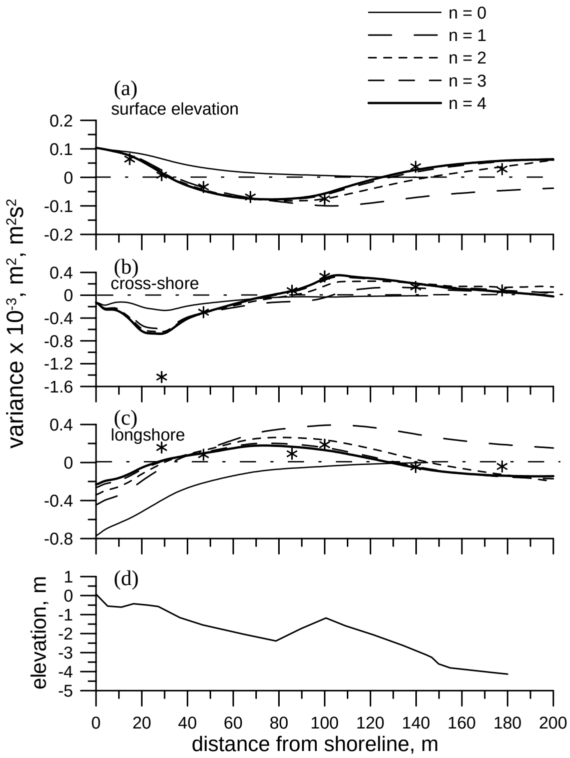

Fig. 12. Measured (∗) and modelled (lines) surface elevation and velocity variance. $f = 0.025$ Hz, hour 246. The cross-shore profile is shown in panel (d).

current velocities were input to the model. Fig. 12 illustrates observed and modelled infragravity variances across the surf zone for hour 246. Model computations were run for edge wave modes $n = 0$–4. Within the area covered by the figure, the cross-shore structure of $n = 3$, 4 edge waves and leaky waves is indistinguishable. Modelled variance was scaled to provide the best overall fit with the observed variance. Correlation between observed and modelled data was slightly better for edge waves opposing the current than for the case with no currents. The correspondence between observed and theoretical cross-shore structure is quite good, except for the large observed cross-shore velocity variance at S7 and model-predicted locations of nodes in velocity and surface elevation agree closely with those observed (see also Fig. 8). Furthermore, Fig. 12 suggests that the infragravity motion at 0.025 Hz may have been an edge wave of mode 3 or higher (or a leaky mode wave) as lower edge wave modes would have had surface elevation nodes seaward, instead of shoreward of S2.

Table 1
Phase relationships between cross-shore (u) and longshore (v) orbital velocity, and surface elevation (η) for the frequency band $f = 0.024$–0.025 Hz at station S6

Hour	u–η	u–v	v–η
239	80 (0.28)	— (0.12)	— (0.01)
241	92 (0.32)	— (0.16)	120 (0.18)
242	83 (0.60)	— (0.08)	— (0.04)
243	83 (0.32)	— (0.03)	— (0.02)
244	98 (0.40)	160 (0.20)	— (0.12)
245	101 (0.50)	— (0.05)	— (0.15)
246	81 (0.61)	161 (0.27)	92 (0.26)
248	79 (0.36)	— (0.12)	— (0.02)
249	92 (0.77)	166 (0.25)	96 (0.18)
250	87 (0.52)	— (0.06)	— (0.12)
251	80 (0.52)	160 (0.21)	105 (0.22)
252	78 (0.48)	163 (0.24)	80 (0.22)
253	77 (0.66)	— (0.09)	— (0.12)
254	83 (0.63)	172 (0.20)	88 (0.17)
256	74 (0.51)	— (0.40)	— (0.10)
258	76 (0.40)	— (0.09)	89 (0.18)

Values are stated in degrees. Coherence-squared estimates are listed in parentheses. The significance level ($\alpha = 0.01$) on coherence is 0.17 (Emery and Thomson, 2001).

The infragravity waves at $f \approx 0.025$ Hz were consequently either primarily longshore progressive or standing edge waves, or leaky mode waves. Such wave motions can only be confidently separated by computing frequency-wave number spectra based upon longshore instrument arrays (e.g. Huntley et al., 1981; Oltman-Shay and Guza, 1987; Howd et al., 1991). In the absence of such an array, we resort to examining the local phase relationships at single instrument locations (Huntley and Bowen, 1978). For such computations, an instrument station is required which is located away from velocity or surface elevation nodes as the coherence between spectral components is likely to be very small at such positions. Furthermore, a location relatively close to the beach is presumed to be advantageous as spectral contamination from, e.g. progressive incident bound long waves is likely to be minimized here due to wave breaking. Consequently, we have selected station S6 on the seaward slope of the inner bar. Table 1 lists local phase relationships at $f = 0.025$ Hz for the storm peak (hours 239–258) at this station. Only cases when the coherence between spectral components were statistically significant ($\alpha = 0.01$) are shown. Phases between cross-shore velocity (u) and surface elevation (η), as well as between longshore velocity (v) and η were generally close to quadrature while the phase-shift between the u and v components was close to 180° at the times when it was significant. Such relationships are indicative of longshore standing edge waves (Huntley and Bowen, 1978).

8. Causes for frequency selection

Profiles exhibiting the configuration required by the cut-off model (Huntley, 1976), i.e. $\beta = 0$ at $x > x_0$ are not commonly observed, but the bathymetry at Staengehus does approximate such a profile configuration (Fig. 1). In Fig. 13, the numerically computed edge wave dispersion curves are shown as well as f, k_y-solutions corresponding to $C = (gh_0)^{\frac{1}{2}}$, where h_0 is water depth at the slope break ($h_0 = 8.16$ m yielding $C = 8.95$ m/s during hour 246). Here, k_y refers to cyclic wavenumber, $1/L_y$. Cut-off frequencies/wave numbers for edge wave modes $n = 1$–6 are shown by dots in Fig. 13. The computed cut-off frequency for an $n = 3$ edge wave is 0.025 Hz, exactly corresponding to the observed amplified frequency.

If the amplified edge waves were indeed the $n = 3$ cut-off mode, it is unclear why only this mode was selected instead of all cut-off modes. A reasonable assumption would be that some of the modes fit the bathymetry and cross-shore forcing structure better than others and that these modes are preferentially forced (Symonds and Bowen, 1984; Bryan and Bowen, 1996). The upper panel of Fig. 14 illustrates computed normalized surface elevation profiles for edge wave modes $n = 1$–3 at theoretical cut-off frequencies. It is evident that the mode 1 wave has a poor overall fit with the bathymetry shown in the bottom panel as it has a surface elevation node at the crest of the middle bar and a large unconstrained antinode over the outer bar. The $n = 2$ wave has a broad antinode over the middle bar but a node at the outer bar crest. Visually it appears that the mode 3 edge wave provides the best overall fit with the bathymetry having antinodes at, or slightly landward of, the crests of the prominent middle and outer bars.

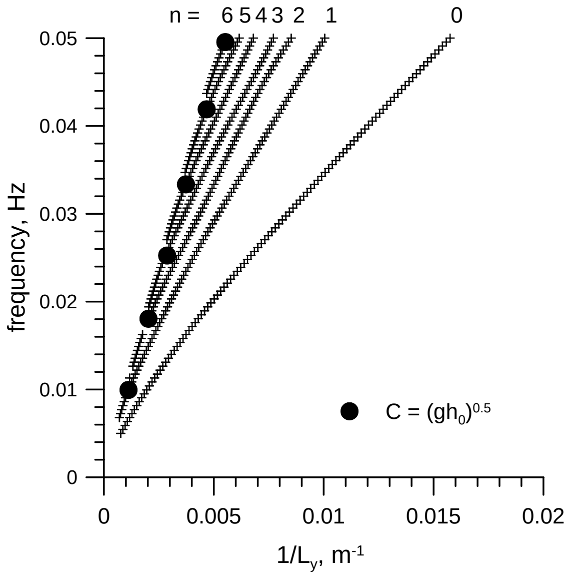

Fig. 13. Theoretical edge wave dispersion curves ($n = 0$–6) for Staengehus. Cut-off frequencies corresponding to $C = (gh_0)^{\frac{1}{2}}$ are indicated by dots.

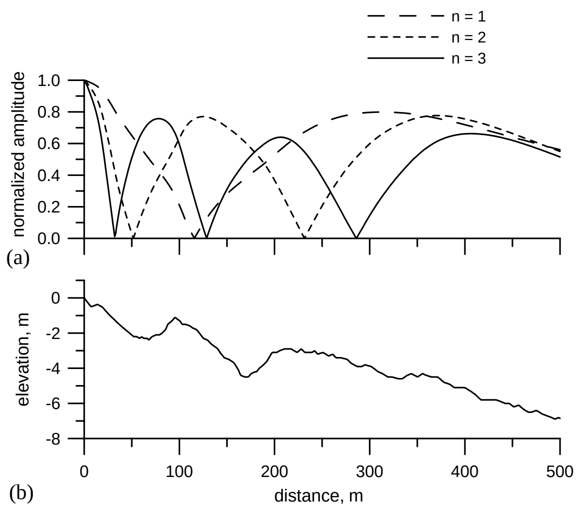

Fig. 14. (a) Normalized surface elevation profiles of edge wave modes $n = 1$ (long dashes), $n = 2$ (short dash) and $n = 3$ (solid line) at cut-off frequencies. Profile bathymetry is shown in panel (b) for comparison.

Some caution should be exercised in the interpretation of these wave shapes as Guza and Inman (1975) pointed out that the cross-shore shape of cut-off modes will deviate somewhat from normal edge waves and develop a long exponential tail in the outer third of the sloping profile segment, i.e. seaward of $x \approx 335$ m in the present case. This region is, however, considerably seaward of the outer bar crest and the instrument array deployed here is unable to distinguish between cut-off waves and 'normal' edge wave shapes.

9. Discussion and conclusions

Statistically significant spectral peaks were observed during the storm at Staengehus at a frequency $f = 0.024$–0.025 Hz. These wave motions were cross-shore standing (Figs. 7 and 8) and had a distinct surface expression (Fig. 6). Based on this evidence, energy at $f = 0.024$–0.025 Hz was in all likelihood due to standing infragravity waves, and not due to shear waves.

The available data suggest that infragravity wave-frequency selection did exist at $f = 0.024$–0.025 Hz for a significant length of time during the storm at Staengehus. The strongest evidence for such a frequency selection was obtained at the most landward instruments, where spectral peaks were observed at frequencies which had all zero-crossings in surface elevation/cross-shore velocity located seaward of the instruments (Fig. 10a and b). Therefore, the observed spectral peaks at these stations could not have been due to an artificial spectral structure imposed by a white-noise shoreline spectrum (i.e. a broad-banded infragravity wave field); the observed peaky spectral shapes were very different from the (local) shapes of the white-noise spectra which did not exhibit peaks at any frequency. This evidence was supported by data from stations located further seaward where spectral peaks were observed at frequencies which were different from those predicted assuming a broad-banded wave field. The excess-variance spectra (Fig. 11) indicate that the frequency selection may have persisted through a period of approximately 20 h during the storm peak. However, given the uncertainties of modelling and spectral interpretation, the present observations must still be considered suggestive.

The cross-shore structures of η, u and v were consistent with theoretical edge wave structures computed from the numerical model (Fig. 11). Locations of zero-crossings suggest that the (edge) waves identified were of mode $n = 3$, or higher. Although firm conclusions can not be reached due to the lack of an alongshore instrument array, local phase relationships indicated that the observed waves were standing edge waves (Table 1).

The study therefore corroborates earlier findings by Aagaard (1990) and Aagaard et al. (1994) who, in previous experiments at the same site, observed dominant infragravity frequencies around $f = 0.02$ Hz in swash and surface elevation spectra and argued that edge wave frequency selection probably existed for this particular beach and that such amplified edge waves generally had frequencies on the order of 0.02 Hz. The conclusions reached during these earlier experiments were, however, based on few data, an assumption of a planar sloping beach in computations of edge wave structure and synthetic spectra were not computed for comparison.

The reasons for the apparent selection of a discrete infragravity frequency are not entirely clear and several mechanisms could be involved. This study has explored the ideas addressed by Huntley (1976) according to which infragravity wave-frequency selection may be due to a modal/frequency cut off imposed by the cross-shore profile shape. Compared to this earlier work, the present results were obtained from a larger number of sensors during high-energy conditions when edge wave amplitudes are relatively large, and in a setting where tides do not significantly shift the position of the shoreline. Consequently, longer data records could be obtained. In addition, edge wave shapes were computed using the existing bathymetry instead of assuming a linear or an exponential cross-shore profile shape.

The observed spectral peak frequency did correspond to the theoretical frequency of the $n = 3$ cut-off mode (Fig. 13), and the modal number of this inferred cut-off mode matched the modal number inferred from the observed and modelled cross-shore structure (Fig. 12). Whether the observed infragravity edge waves were actually cut-off modes cannot, however, be verified, partly because instruments were not deployed in the outermost part of the profile. If that was indeed the case, the restriction on the number of modes at a given time may have been due to constraints imposed by the incident wave field and/or the bathymetry. Fig. 14 shows that the correspondance between the prevailing bar topography and the edge wave shape ($n = 3$; $f = 0.025\,\text{Hz}$) was quite good with edge wave antinodes located at bar crests where the majority of the edge wave forcing due to wave breaking is expected to occur. As earlier suggested by Symonds and Bowen (1984) and Lippmann et al. (1997), it is therefore possible that the bathymetry at Staengehus discriminates against (cut-off?) edge waves whose cross-shore shape does not approximate the cross-shore bathymetric profile.

Acknowledgements

The field work was supported by the Danish Natural Sciences Research Council, grant no. 9701836 and KRB was funded by the Foundation for Research Science and Technology of New Zealand, contract #C01X0015. Brian Greenwood, Jørgen Nielsen, Ulf Thomas, Kalle Kronholm and Rasmus Nellemann Nielsen assisted in the field. Thanks to you all for the many convivial hours spent on the beach. We appreciate the assistance rendered by the North Zealand Forest District (K. Mortensen) and by the Melby Barracks. We appreciate the comments of Professor D.A. Huntley and the anonymous reviewers, whose comments significantly improved the contents of the paper.

References

Aagaard, T., 1990. Infragravity waves and nearshore bars in protected, storm-dominated coastal environments. Marine Geology 94, 181–203.

Aagaard, T., Greenwood, B., 1994. Suspended sediment transport and the role of infragravity waves in a barred surf zone. Marine Geology 118, 23–48.

Aagaard, T., Nielsen, N., Nielsen, J., 1994. Cross-shore structure of infragravity standing wave motion and morphological adjustment: an example from northern zealand, denmark. Journal of Coastal Research 10, 716–731.

Ball, F.K., 1967. Edge waves in an ocean of finite depth. Deep-Sea Research 14, 79–88.

Bauer, B.O., Greenwood, B., 1990. Modification of a linear bar-trough system by a standing edge wave. Marine Geology 92, 177–204.

Beach, R.A., Sternberg, R.W., 1991. Infragravity driven suspended sediment transport in the swash, inner and outer-surf zone. Proceedings Coastal Sediments '91. American Society of Civil Engineers, New York, pp. 114–128.

Bowen, A.J., 1980. Simple models of nearshore sedimentation: beach profiles and longshore bars. In: McCann, S.B. (Ed.), The Coastline of Canada. Geological Survey of Canada, Paper 80–10, pp. 1–11.

Bowen, A.J., Guza, R.T., 1978. Edge waves and surf beat. Journal of Geophysical Research 83, 1913–1920.

Bowen, A.J., Inman, D.L., 1971. Edge waves and crescentic bars. Journal of Geophysical Research 76, 8662–8671.

Bryan, K.R., Bowen, A.J., 1996. Edge wave trapping and amplification on barred beaches. Journal of Geophysical Research 101, 6543–6552.

Bryan, K.R., Bowen, A.J., 1998. Bar-trapped edge waves and longshore currents. Journal of Geophysical Research 103, 27867–27884.

Bryan, K.R., Howd, P.A., Bowen A, J., 1998. Field observations of bar-trapped edge waves. Journal of Geophysical Research 103, 1285–1305.

Eckart, C., 1951. Surface waves on water of variable depth. Scripps Institution of Oceanography, Wave Report 100, Ref. 51–12.

Emery, W.J., Thomson, R.E., 2001. Data Analysis Methods in Physical Oceanography, 2nd Edition. Elsevier, Amsterdam, 638pp.

Gallagher, B., 1971. Generation of surf beat by non-linear wave interactions. Journal of Fluid Mechanics. 49, 1–20.

Guza, R.T., Inman, D.L., 1975. Edge waves and beach cusps. Journal of Geophysical Research 80, 2997–3012.

Guza, R.T., Thornton, E.B., 1982. Swash oscillations on a natural beach. Journal of Geophysical Research 87, 483–491.

Guza, R.T., Thornton, E.B., 1985. Observations of surf beat. Journal of Geophysical Research 90, 3161–3172.

Herbers, T.H.C., Elgar, S., Guza, R.T., O'Reilly, W.C., 1995. Infragravity-frequency (0.005–0.05 Hz) motions on the shelf. Part II: Free waves. Journal of Physical Oceanography 25, 1063–1079.

Holland, K.T., Holman, R.A., 1999. Wavenumber-frequency structure of infragravity swash motions. Journal of Geophysical Research 104, 13479–13488.

Holman, R.A., Bowen, A.J., 1979. Edge waves on complex beach profiles. Journal of Geophysical Research 84, 6339–6346.

Holman, R.A., Bowen, A.J., 1982. Bars, bumps and holes: models for the generation of complex beach topography. Journal of Geophysical Research 87, 457–468.

Howd, P.A., Bowen, A.J., Holman, R.A., Oltman-Shay, J., 1991. Infragravity waves, longshore currents and linear sand bar formation. Proceedings Coastal Sediments '91. American Society of Civil Engineers, pp. 72–84.

Howd, P.A., Bowen, A.J., Holman, R.A., 1992. Edge waves in the presence of strong longshore currents. Journal of Geophysical Research 97, 11357–11371.

Huntley, D.A., 1976. Long-period waves on a natural beach. Journal of Geophysical Research 81, 6441–6449.

Huntley, D.A., Bowen, A.J., 1978. Beach cusps and edge waves. Proceedings 16th Coastal Engineering Conference. American Society of Civil Engineers, pp. 1378–1393.

Huntley, D.A., Guza, R.T., Thornton, E.B., 1981. Field observations of surf beat. 1 Progressive edge waves. Journal of Geophysical Research 86, 6451–6466.

Kirby, J.T., Dalrymple, R.A., Liu, P.L.F., 1981. Modification of edge waves by barred-beach topography. Coastal Engineering 5, 35–49.

Lippmann, T.C., Holman, R.A., Bowen, A.J., 1997. Generation of edge waves in shallow water. Journal of Geophysical Research 102, 8663–8679.

Lippman, T.C., Herbers, T.H.C., Thornton, E.B., 1999. Gravity and shear wave contributions to nearshore infragravity motions. Journal of Physical Oceanography 29, 231–239.

Longuet-Higgins, M.S., Stewart, R.W., 1962. Radiation stress and mass transport in gravity waves, with application to surf beats. Journal of Fluid Mechanics 13, 481–504.

Munk, W.H., 1949. Surf beats. EOS, Transactions AGU 30, 849–859.

Oltman-Shay, J., Guza, R.T., 1987. Infragravity edge wave observations on two california beaches. Journal of Physical Oceanography 17, 644–663.

Oltman-Shay, J., Howd, P.A., 1993. Edge waves on nonplanar bathymetry and alongshore currents: a model and data comparison. Journal of Geophysical Research 98, 2495–2507.

Ruessink, B.G., 1998. The temporal and spatial variability of infragravity energy in a barred nearshore zone. Continental Shelf Research 18, 585–605.

Ruessink, B.G., Kleinhans, M.G., van den Beukel, P.G.L., 1998. Observations of swash under highly dissipative conditions. Journal of Geophysical Research 103, 3111–3118.

Russell, P.E., 1993. Mechanisms for beach erosion during storms. Continental Shelf Research 13, 1243–1265.

Sallenger, A.H., Holman, R.A., 1987. Infragravity waves over a natural barred profile. Journal of Geophysical Research 92, 9531–9540.

Short, A.J., 1975. Multiple offshore bars and standing waves. Journal of Geophysical Research 80, 3838–3840.

Symonds, G., Bowen, A.J., 1984. Interactions of nearshore bars with incoming wave groups. Journal of Geophysical Research 89, 1953–1959.

Symonds, G., Huntley, D.A., Bowen, A.J., 1982. Two-dimensional surf beat: long wave generation by a time-varying breakpoint. Journal of Geophysical Research 87, 492–498.

Ursell, F., 1952. Edge waves on a sloping beach. Proceedings Royal Society of London A314, 79–97.